Effects of shoal margin collapses on the morphodynamics of a sandy estuary

W. M. van Dijk[1], M. R. Hiatt[1,2], J. J. van der Werf[3,4], and M. G. Kleinhans[1]

[1]Department of Physical Geography, Faculty of Geosciences, Utrecht University, Utrecht, The Netherlands
[2]Department of Oceanography and Coastal Sciences, College of the Coast and Environment, Louisiana State University, Baton Rouge, Louisiana, United States
[3]Department of Marine and Coastal Systems, Deltares, Delft, The Netherlands
[4] Department of Water Engineering and Management, Faculty of Engineering Technology, University of Twente, Enschede, The Netherlands

Key Points:

- Shoal margin collapses perturb the channel-shoal network of sandy estuaries.
- Disturbances cause long-term morphological changes.
- Disturbances amplify asymmetry and instability at channel junctions.

Corresponding author: Wout van Dijk, `W.M.vanDijk@uu.nl`

Abstract

Shoal margin collapses of several Mm^3 have occurred in the Western Scheldt estuary, the Netherlands, on average five times a year over the last decades. While these collapses involve significant volumes of material, their effect on the channel-shoal morphology is unknown. We hypothesize that collapses dynamicise the channel-shoal interactions, which could impact the ecological functioning, flood safety and navigation in the estuary. The objective is to investigate how locations, probability, type, and volume of shoal margin collapse affect the channel-shoal dynamics. We implemented an empirically-validated parameterization for shoal margin collapses and tested its effect on simulated estuary morphological development in a Delft3D schematization of the Western Scheldt. Three sets of scenarios were analyzed for near-field and far-field effects on flow pattern and channel-shoal morphology: 1) an observed shoal margin collapse of 2014, 2) initial large collapses on 10 locations, and 3) continuous collapses predicted by our novel probabilistic model over a time span of decades. Results show that a single shoal margin collapse only affects the local dynamics in the longitudinal flow direction and dampen out within a year for typical volumes, whereas larger disturbances that reach the seaward or landward sill at tidal channel junctions grow. The direction of the strongest tidally-averaged flow determined the redistribution of the collapsed sediment. We conclude that adding the process of shoal margin collapses increases the channel-shoal interactions and that in intensively dredged estuaries shoal margins oversteepen, amplifying the number of collapses, but because of dredging the natural morphological response is interrupted.

Keywords: estuary; shoal margin collapse; channel-shoal morphodynamics; tidal bars; Western Scheldt

1 Introduction

The process of channel bank failure and collapses of shoal margins has been recognized in estuaries and rivers around the world [*Coleman*, 1969; *Laury*, 1971; *Silvis and De Groot*, 1995; *Torrey*, 1995; *Dunbar et al.*, 1999; *Van den Berg et al.*, 2002; *Beinssen et al.*, 2014] but their effect on long-term morphological development remains unknown. The implementation of channel bank failure in numerical morphodynamic models has been studied more recently [*Kleinhans*, 2010; *Nicholas*, 2013a; *Schuurman et al.*, 2013] but focused on outer cut bank erosion in rivers. Though, channel banks can also collapse at the inner bank of rivers [*Nieuwboer*, 2012], collapses of shoal margins are more often observed at the inner side of a bend in estuaries [*Wilderom*, 1972; *Mastbergen and Van den Berg*, 2003; *Van Dijk et al.*, 2018a]. Because of the relatively large volume of up to several million m^3 that is involved, the associated displaced sediment in the channel perturbs the sediment transport, affecting channel geometry, e.g., the width-depth ratio, and channel dynamics. We hypothesize that such morphological perturbations within the system may amplify the sediment transport in estuaries as much as extreme events imposed in the boundary conditions, indirectly affecting the morphological changes. This is important because morphological models of estuaries invariably evolve towards bar-scale equilibrium [*Van der Wegen and Roelvink*, 2012; *Dam*, 2017]. This means that the channel-shoal dynamics are presently underpredicted because of internal dynamics and disturbances, such as collapses, are not captured in the model.

Effects of disturbances and perturbations on morphology in rivers and estuaries have been studied in the past century. The damping and lag associated with environmental disturbances propagating through a system are determined by the magnitude and timescale of the event [*Paola et al.*, 1992; *Whipple and Tucker*, 1999]. The nonlinear dynamics of sediment transport limits the potential to record and pass on physical environmental disturbances and perturbations [*Jerolmack and Paola*, 2010]. Such disturbances for fluvial systems have been subdivided into four categories [*Schuurman et al.*, 2016a]: (i) external temporal perturbation of the upstream inflow, (ii) external spatial perturbation, e.g. along the outer channel banks, (iii) external perturbation at the downstream boundary, and (iv) internal perturbations within the reach. Shoal margin collapses fall within the fourth group of disturbances as sediment is eroded from the shoal within the estuary system. Bank erosion results in local widening of the system [*Khan and Islam*, 2003; *Ashworth and Lewin*, 2012], and outer bank erosion is linked to bar (shoal) dynamics, as the eroded sediment is a source for bars [*Xu*, 1997; *Ahktar et al.*, 2011; *Van de Lageweg et al.*, 2014]. This study focuses on the perturbing effects of shoal margin collapses in estuaries, where the flow is bi-directional due to tidal forcing. In tidal systems, flow direction depends on the flood ebb asymmetry within the estuary as well as seasonal influences, particularly in the upper estuary due to higher fluvial flows during large riverine flooding or lower fluvial flows over drier periods.

To study the role of disturbance on the morphology of estuaries, the most control is offered by numerical models. Numerical morphodynamic models are useful tools, but interaction with bank erosion processes introduces complications [*Canestrelli et al.*, 2016]. The forecasting of these interactions is not commonly addressed due to the complexity of coupling short-term geotechnical processes with long-term morphological development. The use of curvilinear grids leads to some complications when modeling abrupt changes such as bank erosion or collapses [*Kleinhans*, 2010], which might be overcome using unstructured grids and cut-cell techniques [*Olsen*, 2003; *Canestrelli et al.*, 2016]. Despite successes in including bank erosion processes [*Darby et al.*, 2002; *Simon and Collinson*, 2002; *Kleinhans*, 2010], erodible floodplains mainly experience outer bank erosion processes [*Nicholas*, 2013a,b; *Schuurman et al.*, 2013, 2016b]. Collapses due to flow slides, such as liquefaction or breaching processes, that also occur on the inner side of bends in estuaries are under-represented. Their potential effects are considerable: a single shoal margin collapse can displace several Mm^3 within hours as observed for the collapse in 2014 in the Western Scheldt [*Van Schaick*, 2015; *Mastbergen et al.*, 2016; *Van den Berg et al.*, 2017; *Van Dijk et al.*, 2018a]. The timing of the collapse determines the response to the event, which is likely to be different around slack water than at peak flow.

Shoal margin collapses through flow slides often occur suddenly, which makes them difficult to predict in current numerical morphodynamic models, such as Delft3D. Shoal margin collapses occur at sufficiently high and steep slopes, but there is a difference in the sediment properties between these two types of flow slides, known as liquefaction and breaching [*Van den Ham et al.*, 2014]. Liquefaction requires loosely packed, non-lithified, and water-saturated sand or silt, whereas breaching requires the presence of a sufficiently large body of densely packed fine sand or silt [*Van den Ham et al.*, 2014]. These short-term processes have been represented by various models but not implemented in a numerical morphodynamic model. *Van den Ham et al.* [2014] argued that these theoretical liquefaction and breaching models quantify the relative influences of channel geometry and soil parameters but the reliability of the estimated probability remains limited. Thus, *Van den Ham et al.* [2014] proposed a semi-empirical model that predicts the probability of shoal margin collapses on profiles, which was modified and extended for application on spatial bathymetry data by *Van Dijk et al.* [2018a]. This predictor includes an empirical factor based on the frequency of historical flow slides in the Eastern Scheldt and Western Scheldt estuaries [*Wilderom*, 1979; *Van Dijk et al.*, 2018a], which is applied in this study instead of the full process-based modeling of flow slides.

Our objective is to increase understanding of the interactions between shoal margin collapses and the channel dynamics of a sandy estuary, the relevant timescales, and the large-scale morphological effects. The posed research questions are: (i) what are the local (near-field) effects of individual shoal margin collapses, such as the observed 2014 shoal margin collapse? (ii) How do multiple shoal margin collapses affect the channel dynamics of the estuary (far-field effect)? Our method was to use the numerical morphodynamic model Delft3D and implement an effective parametrization for the process of shoal margin collapses in a calibrated model. We then tested how disturbances, such as multiple collapses, propagate and change the channel-shoal interactions of the Western Scheldt, a sandy estuary. In this paper, we first give a detailed description of the study area, the method for implementation of the shoal margin collapses in Delft3D and the tested scenarios. Then, we present the near-field and far-field effects of shoal margin collapses on the short-term as well as the long-term morphodynamics of the Western Scheldt. Finally, we discuss the model performance and the implications of persistent perturbations on a sandy estuary.

2 Study Area

This study focuses on shoal margin collapses in the Western Scheldt. The Western Scheldt is located in the southwestern part of the Netherlands (51°41’51"N, 5°40’35"E) and is the seaward section (60 km) of the 200 km tide-dominated Scheldt estuary. The Scheldt is a well-studied and monitored estuary [e.g., *Wang et al.*, 1999; *Winterwerp et al.*, 2000; *Bolle et al.*, 2010; *Van der Wegen and Roelvink*, 2012] that provides access to various harbors, of which the port of Antwerp (Belgium) is the largest. The Western Scheldt is characterized by a convergent geometry and has a well-developed system of channels and shoals (Figure 1a).

Channel bank failures have been recorded systematically in the Western Scheldt for the past 200 years [*Wilderom*, 1961, 1979]. Over the years, bank protection measures have been implemented to protect the channel banks and dikes of the Western Scheldt against new failures and collapses. Yet, these measures did not prevent the occurrence of shoal margin collapses [*Wilderom*, 1972]. A recent study identified 300 shoal margin collapses between 1959-2015 [Figure 1a, *Van Dijk et al.*, 2018a], ranging from very small collapsed volumes of 20,000 m^3 up to volumes of 3,000,000 m^3. The majority of the collapses occur at unprotected areas. The estuary consists of relatively fine sediment, which affects the occurrence of shoal margin collapses [*Van den Ham et al.*, 2014]. In general, the D_{50} of the channel bed varies between about 200 μm and 300 μm, whereas at the higher elevation areas of the shoals the sediment size is generally finer than 200 μm [*Cancino and Neves*, 1999; *De Vriend et al.*, 2011]. Additionally, a significant percentage of mud, up to 25%, is found in the inter-tidal areas but increases above 25% on the flanks of the estuary [*Braat et al.*, 2017; *Van de Lageweg et al.*, 2018].

The natural development of the morphology, as well as the effect of perturbations, is the result of interactions between water flow, sediment transport, and bed elevation. An important factor causing bi-directional flow and mean sediment transport is the tidal forcing in the Western Scheldt [*Wang et al.*, 1999]. From the mouth of the estuary to the Dutch/Belgian border, the tidal range increases from 3.5 m to 5 m [*Jeuken*, 2000]. The tidal prism at the mouth is about two billion m^3 [*Wang et al.*, 1999], whereas the yearly-averaged river discharge of the Scheldt into the Western Scheldt is a negligible 120 m^3/s [*Cancino and Neves*, 1999; *De Vriend et al.*, 2011] but peak discharges are observed up to 600 m^3/s [*Baeyens et al.*, 1997]. The Western Scheldt has several re-circulation zones of sediment through the ebb and flood channels, which enclose the inter-tidal flats [Figure 1b, *Wang et al.*, 1995; *Winterwerp et al.*, 2000]. The tidal flow is asymmetric, i.e., slower but longer ebb flows compared to flood flows (Figure 1c–d). The difference between the maximum flow velocity for ebb and flood illustrated that the flood is generally stronger (Figure 1e) even in the ebb dominated channels as illustrated by the tidally-averaged flow (Figure 1b).

3 Model description and methods

3.1 Model setup and boundary conditions

In this study, we used two Delft3D schematizations that are both based on the NeVla-Delft3D model of the Scheldt estuary, which includes the upstream Flemish branches of the estuary, the Western Scheldt and part of the North Sea. The NeVla model is a state-of-the-art numerical model that has been optimized for hydrodynamics [*Maximova et al.*, 2009a,b,c; *Vroom et al.*, 2015] and morphology [*Grasmeijer et al.*, 2013; *Schrijvershof and Vroom*, 2016]. To study the effect of shoal margin collapses we focused on the Western Scheldt part of the NeVla model. Two nested models were produced from the NeVla-Delft3D model for reducing the computational time.

The first nested model boundaries (model 1) were located around the tidal flat of Walsoorden (see boundaries in Figure 1a), which was used to study the morphodynamic response of the 2014 shoal margin collapses and the sensitivity to collapse sizes, grain-size of the collapsed material, and location of the collapsed deposits. *Van Schaick* [2015] validated the water level and discharge from the nested model with the NeVla-Delft3D model as well as the response of the 2014 collapse, and concluded that the errors were small enough to be neglected for the area of interest.

The second nested model boundaries (model 2) include the Western Scheldt from the mouth at Vlissingen to the Dutch/Belgian border (see seaward boundaries in Figure 1a), which was used for testing the effect of shoal margin collapse locations as well as the effect of multiple shoal margin collapses in the Western Scheldt over time. The downstream boundary was chosen at the smallest but deepest part of the Western Scheldt to limit boundary effects. Still, we excluded the seaward effects for further interpretation and conclusions as it was difficult to distinguish the boundary effects from an effect associated to the actual collapses. A single spring-neap-spring cycle shows that the tidally-averaged flow of this model (Supplementary Figure S4b) is comparable with the outcome of the full NeVla-Delft3D model (Figure 1b), except for a small variation at the seaward end.

The nested model consists of a curvilinear grid with various grid sizes. The boundary conditions include a water level fluctuation due to tides at the seaward boundary and current at the landward boundary. Sediment fraction was uniform, with a median grain-size of 200 μm. For simplification, the boundary conditions were selected from a single spring-neap-spring tide cycle of January 2013 (about 14 days) and repeated for a 2 year period. Furthermore, we excluded the wind direction and magnitude from the NeVla model to reduce computational time because the effect of wind is negligible within the Western Scheldt. The roughness field in the model is defined in Manning n and is variable over the model domain [*Maximova et al.*, 2009a,b,c; *Vroom et al.*, 2015], which was 0.022 $\mathrm{s{\cdot}m^{-1/3}}$ for the eastern part, 0.027 $\mathrm{s{\cdot}m^{-1/3}}$ for the western part and 0.028 $\mathrm{s{\cdot}m^{-1/3}}$ for the Verdronken Land van Saeftinghe. The bed consisted of erodible and non-erodible layers [*Gruijters et al.*, 2004], the non-erodible layers formed due to previous deposits that are hardly erodible [*Dam*, 2013], and so the sediment thickness varies within the Western Scheldt model (Supplementary Figure S1). Because sediment transport was calculated by *Van Rijn* [2007a,b], the bedload and suspended load transport could be separated.

3.2 Transverse bed slope and morphological factor

The Delft3D model (version FLOW 6.01.07.3574, 2 April 2014) has been applied in many scientific projects to compute hydrodynamics, sediment transport, and morphological changes [*Roelvink*, 2006; *Deltares*, 2009; *Crosato and Saleh*, 2011; *Van der Wegen and Roelvink*, 2012; *Schuurman et al.*, 2013, 2016a; *Van Dijk et al.*, 2014]. In this study, we applied a 2D depth-averaged flow field, which meant that the effect of helical flow driven by flow curvature on bed shear-stress direction was parametrized [*Schuurman et al.*, 2013; *Baar et al.*, 2018a,b]. The parametrization affected the transverse bed slopes at the shoal margins, which influenced the moment that shoal margin collapses were predicted. We performed a sensitivity analysis to determine how the sediment transport direction affects the slopes for α_{bn} between 1.5 and 100 [see Supplementary Text S1, *Bagnold*, 1966; *Ikeda*, 1982a,b; *van Rijn*, 1993]. To reduce computational time, Delft3D includes a morphological acceleration factor M. Based on a sensitivity analyses (see Supplementary Text

S1) we set α_{bn} to 30 and M to 20 as a default, so that that realistic dimensions of the slopes for long-term simulations were maintained (Supplementary Figure S2).

3.3 Model scenarios and sensitivity

We assessed the effect of shoal margin collapses on the morphodynamics of a sandy estuary in three scenarios (see Table 1). We compare each scenario with a control run without collapses, so that natural variation of the morphodynamics by the model could be excluded and check if collapses dynamicise the model.

The first scenario focused on understanding the near-field effect of a single shoal margin collapse, such as the observed 2014 shoal margin collapse at the tidal flat of Walsoorden. The sensitivity of the shoal margin collapse size, location of the collapsed deposits, and grain-size of the deposits were studied (see Supplementary Text S3). The sensitivity scenarios of the size and the location are based on the evaluation of historical collapses by *Van Dijk et al.* [2018a]. The grain size of the deposited material was varied as the grain-size distribution in the field showed minor variation between 100 μm on the shoals and 300 μm in the channel [*Mastbergen et al.*, 2016]. The first scenario and sensitivity tests were conducted on only the eastern part of the Western Scheldt (see the seaward boundary of model 1 in Figure 1a).

The second scenario included a model run with initially 10 shoal margin collapses of 1,000,000 m^3 located at various locations within the Western Scheldt. Here, we tested the far-field effect on the sediment transport and channel-shoal dynamics over the long-term (40 years). The locations corresponded to observed shoal margin collapse locations as described in *Van Dijk et al.* [2018a] (Figure 1a).

The third scenario tested the role of multiple shoal margin collapses over a period of 40 years, where multiple collapses occurred within one year, hereafter referred to multiple yearly collapses. These collapses were controlled by the implementation of our novel shoal margin collapse rules in a Matlab environment as described in the next section. These last two scenarios were applied on a different nested model (see Table 1), which includes the Western Scheldt from Vlissingen to the Dutch/Belgian border (see the seaward boundary of model 2 in Figure 1a).

3.4 Shoal margin collapses

Including the process of shoal margin collapses into a morphodynamic model might be necessary to increase dynamics within the model domain, such as the channel-shoal interactions. Currently, bank erosion is implemented by coupling horizontal bank retreat to bed degradation in Delft3D. Bank erosion occurs between an inundated grid cell and a dry grid cell, and thus is not restricted to the outer banks. Incision of the inundated grid cell could be equally divided over both grid cells or solely on the dry cell, so that the dry cell was lowered and the bank eroded [*Schuurman et al.*, 2016b; *Mastbergen and Schrijvershof*, 2016]. This process continues until the grid cell becomes inundated, but shoal margin collapses may occur suddenly at growing shoals that become less inundated.

In this study, shoal margin collapses are enforced based on the historical evaluation of collapses in the Western Scheldt and the adapted forecasting method by *Van Dijk et al.* [2018a]. The first step towards implementation is by determining the inter-tidal shoals and their margins using the method of *Leuven et al.* [2018a] by fitting a linear regression for the median bed elevation along the estuary channel. Elevation above the regression line was interpreted as a shoal and below as a channel. The boundary of the shoal was then extracted to determine the shoal margin. Subsequently, shoal margin collapse frequencies, F_{SC}, were calculated [adapted from *Van Dijk et al.*, 2018a] as follows

$$F_{SC} = \left[\left(\frac{H}{11} \right)^{2.5} \left(\frac{9.5}{\cot\alpha} \right)^{5} \right] \frac{SC_{avg}}{L_{sm}} \tag{1}$$

where H is the elevation of the local maximum between the center and the deepest part within a window size of 300 by 300 m on a 20 by 20 m interpolated grid of the bed elevation. α is the corresponding angle to H, SC_{avg} is an empirical value based on the average number of collapses observed per year [5.3 for the Western Scheldt, *Van Dijk et al.*, 2018a], and L_{sm} is the measured total length of shoal margins [300 km for the Western Scheldt, *Van Dijk et al.*, 2018a]. The form of equation 1 allowed the frequency of collapse to be greater than 1, which was prevented by a transformation, namely a Poisson process, of the frequency into a probability (P_{SC}):

$$P_{SC} = 1 - e^{-F_{SC}} \tag{2}$$

Van Dijk et al. [2018a] found that at a probability threshold (P_{SC}) value of 10^{-4}, the true positive rate, defined as the number of cells that had shoal margin collapses in both the predictive probability and observed collapses divided by the number of observed locations of collapses, was almost 0.5. At this probability threshold, the remaining predicted shoal margin collapse locations show a low false positive rate, which is defined as the number of cells that had shoal margin collapses in the predictive probability but no observations of collapses divided by the number of cells with no shoal margin collapse observations. Because multiple locations at the shoal margin could have a probability value greater than the given threshold of 10^{-4}, we capped the number of collapses to a maximum of 1 per tidal flat (shoal margin) per time-interval. This means that per time-interval only a maximum of 8 collapses can occur along the Western Scheldt. The time-interval was set to one morphological year. Eroding shoal margins were excluded, because these were already eroding by continuous channel migration, and collapses mostly occurred suddenly at vertical aggradational margins. The highest probability above the critical probability of 10^{-4} was used to select the location of the shoal margin collapse per tidal flat. These slopes collapsed to a post-event slope whilst conserving mass, in which the size and geometric shape of the collapses followed a 1/3 ellipsoid according to the analysis of *Van Dijk et al.* [2018a] of the geometric shape of the erosion scar (see Supplementary Text S2).

3.5 Data analyses

The Delft3D model outcomes were analyzed for near-field and far-field effects, i.e., local and estuary scale. The analysis of the near-field effects on a short-term was conducted on the first scenario, whereas for the Western Scheldt model (second and third scenario) the far-field effect on the long-term morphology was analyzed. For the near-field effect, we analyzed the distribution of the collapsed sediment by labeling the collapsed deposit as a second sediment fraction with the same grain-size in the model. The model outcomes were also analyzed by looking at the Digital Elevation Model (DEM) of Difference (DoD) between a run with the collapse and the control run. The distribution of the collapsed sediment was plotted in a time-space diagram for the cross flow-direction as well as longitudinal flow-direction. Furthermore, the width-averaged bed elevation was calculated on the channel centerline-normal transects and compared between the runs with and without collapses.

For analyzing the shoal margin collapse effects, the tidally-averaged flow and mean sediment transport were calculated over a spring-neap-spring tidal cycle, starting and stopping at the same water level point. The tidally-averaged flow and mean sediment transport were summarized by plotting the vectors for determining the net direction of the flow and of the sediment transport. For the second scenario, the sediment transport direction was determined for the spring-neap-spring tidal cycle at the 10 locations of the collapsed scar and associated deposit and plotted in a rose diagram. Smoothing of the bed elevation after the collapse was determined by calculating the average bed elevation within the scar and the associated deposit locations.

We were specifically interested in the role of shoal margin collapses on the channel-shoal interactions. Thus, we used an existing network extraction tool to characterize the channel dynamics. This tool has been applied to braided rivers to determine the drainage network, so it includes channel bifurcations and confluences [*Kleinhans et al.*, 2017]. The tool uses the local lows of the channel bed to determine its lowest path. Specifically, the tool determines minimums, maximums and saddle points and connects the minimums through a saddle point, according to a descending quasi Morse-Smale complex [*Kleinhans et al.*, 2017]. Besides the lowest path, the algorithm computes a complete set of paths that form the entire channel network. To achieve this, an ordered set of non-crossing paths, known as striation, are computed. To do this, the DEM is split around the lowest path π into two parts. Then the lowest paths in those two parts of the DEM are found, and the DEM is split around these paths, and so on. This continues until a threshold, referred to as a sand function (δ), is reached. The sand function is defined as the summation of the volume of sediment that has to be removed before two channels become one in the network. The volume of sediment is calculated from the elevation above the saddle point [Figure 2b, *Kleinhans et al.*, 2017]. This made it possible to compute graphs representing the channel network, consisting of the lowest paths for ‘sufficiently different‘ scales (Figure 2c).

Three threshold values for δ were chosen, representing three different network scales. The networks scales are similar to the names used in the Western Scheldt [*Jeuken*, 2000]. But, there is a mismatch between extracted channels from the network tool and field observations. The largest scale is the main channel, the next scale is the secondary channel, and the third scale is the connecting channel. In nature, the connecting channel connects the secondary channel to the main channel. We used the channel network to analyze the channel depths for the three network scales and between model outcomes.

4 Results

4.1 The 2014 shoal margin collapse

4.1.1 Hydrodynamics

Changes in bed elevation and associated bed friction due to a shoal margin collapse affected the water level around the collapse as well as the associated deposit. Over time, the water level fluctuates within 1 cm between scenario 1 and the control run under the same boundary conditions (Figure 3a, b). The main water level difference is noted in the transverse direction of the collapse (Figure 3c,d & g). In the longitudinal direction, there is less water level difference between scenario 1 and the control run (Figure 3e, f). The largest difference in the water level change is observed at the scar of the shoal margin collapse (Figure 3d). Here, the inundated time is longer because of the lower elevation. The two runs do not dominantly show lower or higher water levels. The skewness in the distribution of the water level changes indicates that water level increases for the shoal margin collapse deposit locations (Figure 3c, g). While the other locations show a decrease in the water level. The distribution of the water level changes varies between ebb and flood conditions for locations landward and seaward of the shoal margin collapse (Figure 3e, f), indicating that water level increases for flood conditions seaward and decreases for flood conditions landward.

The small changes in the water levels affected the tidally-averaged flow direction along the shoal margin. The control run shows that the tidally-averaged flow direction (Figure 4a) is comparable with the original NeVla-Delft3D model (Figure 1b) around the tidal flat of Walsoorden. The tidally-averaged flow remains similar for both simulations. The direction and magnitude of the tidally-averaged flow are affected around the location of the collapse. For example, flow velocity increases along the shoal margin with 0.1 m/s because of the collapse (Figure 4b).

4.1.2 Sediment transport

Sediment transport is calculated with the *Van Rijn* [2007a,b] equation, which separates the bedload from suspended load transport. The mean total transport follows the direction of the tidally average flow. On the north side of the channel, the total transport is towards the center (Figure 4c). In the center of the channel, sediment transport is ebb dominated. On the south side of the channel, sediment transport is flood dominated. The mean bedload transport follows the direction of the tidally-averaged flow (Supplementary Figure S5a), which indicates a clear distinction in ebb and flood directed transport. The mean suspended sediment transport does not follow the tidally-averaged flow direction at all locations, especially in the main channel south of the tidal flat of Walsoorden (Supplementary Figure S5b). Here, the direction is in the opposite direction of the bedload transport. Suspended sediment transport is flood directed at the north side of the channel, and ebb directed at the south side. We suspect that this is the result of the transverse bed slope predictor, which has no effect on the suspended sediment transport. The transverse bed slope of α_{bn} of 30 showed a strong transverse direction of the sediment transport (Figure 4c). Analysis of model runs with the default α_{bn} of 1.5 (Supplementary Figure S5d) showed that the magnitude in the longitudinal direction is comparable.

Changes in the tidally-averaged flow due to the shoal margin collapse affected the sediment transport direction and magnitude. The run with the shoal margin collapse of 2014 showed an 80% reduction against the control run for the mean total transport, i.e., the effective sediment, at the deposition location of the collapsed shoal margin (Figure 4d). The mean total transport along the shoal margin increases by 15% and even more within the shoal margin collapse. The decrease in sediment transport means that erosion of the deposited sediment from the collapse will take longer. The increase of sediment transport along the margin increases erosion potential.

4.1.3 Morphodynamics

By comparing scenario 1 to the control run, changes in the morphology between the runs can be ascribed to the shoal margin collapse. The DEM of difference (DoD) shows that the bed elevation in the channel landward as well as seaward of the collapsed deposit is raised after about 1 year of morphological time, whereas the location of the deposit is lowered from the start of the simulation (Figure 4e). This suggests smoothing of the profile after the collapse. The shoal margin collapse scar is still visible in the landscape. The process of sedimentation in the scar is slower than the erosion of the deposited sediment in the channel.

The difference in bed elevation shows the changes between the two runs, but does not show the distribution of the sediment from the collapse. Figure 4f shows the distribution of the labeled sediment from the 2014 collapse around the tidal flat of Walsoorden. Large portions deposited at the sides of the original location, which corresponds with the DoD. The distribution of the collapsed sediments spread over a large area in the landward as well as seaward direction. This was less visible from the DoD because of the modest changes in bed elevation. Suspended sediment transport traveled a longer distance, whereas bedload transport affected bed elevation. Despite the transport in both directions, the dominant distribution of the tracer sediment was in the ebb direction (Figure 4f).

4.2 Shoal margin collapse scenarios to determine sensitivity

In the supplementary, we elaborate in more detail on the sensitivity of various scenarios, such as the size of the collapse, the location of the collapsed sediment and the role of grain-size. The analysis shows that the migration rate of the disturbance is hardly affected by the collapsed volume, and that only large collapses, > 100,000 m^3 affect the far-field channel-shoal interactions (Supplementary Figure S7). This is because the volume of collapsed material is relatively small compared to the characteristic shoal volume of 34 million m^3. The tidally-averaged flow direction at the location of the collapsed deposits determines the dominant direction of the disturbance. Collapses that occurred more landwards are less reworked and the transport direction is dominantly in the seaward direction (Supplementary Figure S7). Model outcomes for different α_{bn} values do not change the longitudinal displacement of the disturbance but do affect the distribution of the sediments in the transverse direction (Supplementary Figure S5c, d). Alongside the location of the collapsed deposit, the grain-size distribution of the deposited sediment also determines the direction of the disturbance. A sand fraction smaller than 200 μm (100 μm) follows the same longitudinal direction as the median sand fraction of 200 μm, but more sediment deposited at the sides of the channel. Sand fraction coarser than 200 μm (300 μm) is, however, transported in the strongest flow direction rather than that of the tidally-averaged flow, so that only the sediment in the deepest part of the channel is entrained (Supplementary Figure S6).

To summarize, shoal margin collapse scars and associated sediment deposits in the channel affect the local dynamics of the Western Scheldt, such as the sediment transport direction and morphology within the first year after the occurrence. Additionally, the size and location of the collapse have direct effects on the magnitude and direction of these dynamics.

4.3 Shoal margin collapses in the Western Scheldt

The 2014 shoal margin collapse is one of the larger collapses that occurred but its effect on the estuary morphodynamics is modest. Here, we first assess how much effect each individual location susceptible to collapse (see specific collapsed locations in Supplementary Figure S4a) has on the morphodynamics. Then, we apply our novel shoal margin collapse parameterization and test if multiple yearly collapses over time would dynamicise the model of the Western Scheldt estuary.

4.3.1 Multiple initial collapses

We used the Western Scheldt schematization (model 2) to test the long-term effect of multiple shoal margin collapses on the morphodynamics of the system. In the first scenario, 10 shoal margin collapses of a volume of 1,000,000 m^3 are added to the initial bed elevation of the Western Scheldt. Sediment transport is dominantly in two directions for most locations, corresponding with the ebb and flood current. The dominant direction differs between the source (scar) and the associated sediment deposit (Figure 5). Generally, the sediment transport is less for the location of the scar compared to the location of the associated sediment deposit. This is particularly true for more landward scars, which becomes dry during low tide. There are some exceptions to this, where the collapse occurs underwater, e.g., the Spijkerplaat (location A), and the scar remains underwater during the tidal cycle. Perpendicular to the ebb and flood flow sediment is transported on the transverse bed slope. A strong perpendicular vector is observed for the collapse at the Molenplaat and Plaat van Walsoorden (locations F and I). This is probably the result of the relatively high value of α_{bn} of 30.

Sediment transport determines the rate at which the shoal margin collapse is filled and the associated collapsed sediment is eroded. The net sediment transport varies between ebb and flood flow as well as between spring and neap tidal cycles. The net sediment transport for a neap tidal cycle is about $5{\cdot}10^5$ m^3 and for a spring tidal cycle about $5{\cdot}10^6$ m^3. The net sediment transport is higher during rising tide than for falling tide. Locations (location A and H) with the highest sediment transport rates show faster infilling of the scar (Figure 6a). The collapse at the tidal flat Walsoorden (location I) is less filled. This is also observed from the first scenario model outcome and corresponds with lower sediment transport rates. Yet, the rate of infilling and erosion deviates from the observations of the 2014 collapse. In general, the filling of the scar is less (Figure 6a). Sediment transport rate also determines the rate of erosion of the collapsed sediment. In general, the erosion is faster than the infilling. There are some exceptions where collapsed deposits are slowly eroded. This applies for the collapses that occurred along the shallower secondary channels (Figure 6b), e.g., the Brouwersplaat (location E) and Molenplaat (location F).

The initial collapses affect the long-term changes of the morphology in the estuary. The sediment transport direction and magnitude at the collapsed locations (Figure 5) determines the distribution of the collapsed sediment and the bed elevation difference (Figure 7a). The bed elevation changed majorly around the shoal margin collapse locations (Figure 7a). Sediment is locally distributed in the landward and seaward direction from its original location. Interesting long-term effects are observed when the disturbances enter areas that accommodate less sediment transport but are morphodynamically active and control sediment division, i.e., the junctions seaward or landward of the channel. Here, the bed elevation is not only affected in the longitudinal direction but also in the transverse direction into connected channels (Figure 7a), i.e., effectively following the sediment vectors. For example, the collapse at location B changes the bed morphology of both landward channels compared to the control run, which also appears at the landward direction of location H (Figure 7a).

On a longer timescale, the shoal margin collapses affect the dynamics of the system. A total volume change of $4.53{\cdot}10^8$ m^3 was observed compared to the control run, in which less than 10% of the volume comes from the initial collapses. The width-averaged mean bed level difference between scenario 2 and the control run shows that changes excite, i.e., grow, over time (Figure 7b). In the beginning, there is a slight difference between the runs, which was also demonstrated with the 2014 collapse. But on the long-term, the mean bed elevation between scenario 2 and the control run varies more than a meter (Figure 7b). This is primarily the result of migration of the junction around location C and landward of location H (Figure 7a). Following the tracer sediment along the estuary gives more insights into the dominant migrating direction of the disturbance (Figure 7c). The dominant direction depends on location, but is generally landwards for the seaward collapses and seawards for the more landward collapses. This corresponds with the dominant sediment transport direction shown in Figure 5. Bed elevation changes even occur in the locations where no sediment originated from the shoal margin collapse is located, e.g., at 25 km (Figure 7b,c). This location corresponds to one of the channel junctions.

4.3.2 Multiple yearly collapses

In the third scenario, shoal margin collapses occurred after each morphological year. The shoal margin collapses vary in size and location according to the given rules (see method section). These rules led to 227 collapses, i.e., 5.7 per year, at 58 independent locations of distinct tidal flats over 40 morphological years (illustrated by contour lines in Figure 8a). A total volume of 40 million m^3, i.e., 1 million m^3 per year, is eroded, which is more than the historical field observations. Previous scenarios show that the distribution of the disturbance varies with location depending on flow conditions (see direction in Figure 1b-e). Again, changes in the bed elevation occur mainly in the longitudinal direction, i.e., landward and seaward of the collapse (Figure 8a). Collapses near the junctions lead to changes in the bed elevation across the channel because the channel is wider and shallower. This occurred at the same locations (B and H) as for the initial collapses, where the bed elevation differs up to 10 m compared to the control run. The total bed volume difference at the end of the model run is $4.63{\cdot}10^8$ m^3 compared to the control run. 20% of the volume comes from the 227 collapses.

The width-averaged bed level difference between scenario 3 and the control run (Figure 8b) illustrates the migration of the disturbance in both directions, excitation of the disturbance over time and also dampening of the disturbance. The bed elevation difference is dampened for the collapses that occurred at 13 km from the seaward end (Figure 8b), whereas migration is detected at 28 km from the seaward end (Figure 8b). Furthermore, there are some unexplained responses that are not associated with the collapses themselves, such as observed between 25 and 37 km from the Western Scheldt mouth, which probably is due to excitation of earlier collapses (Figure 8b). Because of the number of collapses and the yearly adding of new collapses, the effect of a single disturbance is difficult to follow. Most changes occur at the locations with several collapses. The total eroded and deposited volume is $2.31{\cdot}10^9$ m^3 for scenario 3 and $2.26{\cdot}10^9$ m^3 for the control run. This suggests that the simulations are equally dynamic as the difference of 50 million m^3 is explained by the collapsed volume of 40 million m^3.

4.4 Re-organization of the channel-shoal network by collapses

The addition of yearly collapses in the model leads to detected changes in the channel network structure and scale compared to the control run (Figure 9a, b). While the main channel location and scale are generally the same between the three runs over time (Supplementary Figure S8), many of the smaller scale channels are identified differently for the model run with yearly collapses. In the control run, fewer smaller scale channels, i.e. secondary and connecting, are observed compared to the run with yearly collapses (Figure 9a-b). This means there is better connectivity among the channels for the model with yearly collapses. The scale, or sand function volume, at which channels are detected, changes between the runs as well. The shifting of the channel network is associated with the differences in the morphological development of the system. In the case of the collapses, the secondary channel network shifts in space (Figure 9b). Sediment deposition in the channel decreases the volume of sediment between adjacent channels, and so the volume for δ. So that, identified secondary channels in the control run are identified as connecting channels in the run with collapses. Over time, the location of the main channel, associated to channel migration, covers 2% less, whereas the secondary channel covers 4% more of the Western Scheldt in the situation with yearly collapses (Supplementary Figure S8).

The various channel networks are used to determine the depth distribution of the channels. The initial network shows a deep main channel (Table 2, Figure 9c). This deep channel is because of dredging activities for maintaining a specific depth of the shipping fairway in the Western Scheldt. After 40 years of morphological development, the main channel becomes deeper but the variation increases (Table 2), showing deeper but also shallower channels. There is an increase in the number of smaller scale channels (Figure 9d), especially for the run with yearly collapses (Figure 9f). We observed some changes in bed elevation between the control run and the model run with yearly collapses, which has a wider distribution (Figure 9d, f). The main channel depth for the model run with 10 initial collapses is more comparable to the control run (Figure 9d, e). Major changes are observed between the secondary and connecting scale channels, the number of connecting scale channels increases for the run with initial collapses, while the depth generally decreases. The depth of the secondary channel, however, increases for the run with initial collapses. The system with yearly collapses develops to a system with shallower channels because collapses occur primarily in the main channel. The distribution of the secondary channel depths migrates towards the depth distribution of the main channel, whereas the number of connecting channels increases (Figure 9f).

5 Discussion

We introduced an effective parametrization for the process of shoal margin collapse, based on the local bed elevation and slope gradient. Here, we discuss how the response of the modeled collapses affects the morphodynamics and how this differs from observations. We also consider the implication of shoal margin collapses on perturbing the channel-shoal interactions and hypothesize these are comparable to larger perturbations caused by dredging and disposal activities.

5.1 Modeled collapses versus observations

The 2014 shoal margin collapse shows the near-field effects of a single collapse. This collapse is well studied by *Van Schaick* [2015] by analyzing field measurements and Delft3D simulations. *Van Schaick* [2015] concluded that some morphodynamics of the model differs from the observations [*Mastbergen et al.*, 2016]. According to field measurements, sediment deposited from the shoal margin collapse migrated in the flood direction, i.e., flood-directed net bedload, while the model outcome suggests ebb-directed net bedload. The discrepancy in the net bedload direction could be explained by the inaccuracy in the modeled hydrodynamics. The deposit from the 2014 shoal margin collapse is located in that part of the channel where the tidally-averaged flow is ebb dominated but almost zero, whereas south from the deposit the tidally-averaged flow and mean sediment transport suggest transport in the flood direction. Yet, the flood current is generally stronger in the channel, which might have led to the distribution of the deposit in the flood direction instead of the modeled ebb direction. The rate of infilling of erosion scars was less in the model compared to field observations (Fig 6a), whereas the field observation of erosion of the associated deposit compares more closely to the modeled results. The difference indicates that the model has difficulties with the simulation of the shallower regions, maybe because no extreme water level conditions are included (only 1 repeated month of real time-series) nor combined astronomical and meteorological forces [*De Vet et al.*, 2018]. Additionally, filling of the scars increases when a mud fraction is added to the model [*Van Schaick*, 2015].

The shoal margin collapse parametrization leads to several collapses along the Western Scheldt Estuary. The location is based on the bed elevation, such that steep slopes collapse, whereas the collapsed size and volume is randomly drawn from a log-normal distribution. Locations for shoal margin collapses (Figure 8a) do vary from the observed locations (Figure 1a). We expect that for the chosen probability threshold value, the number of false positives is at least equal to the number of true positives. This means that steep high slopes that are not susceptible to collapses are included as well [*Van Dijk et al.*, 2018a]. Nonetheless, the collapses are widely distributed on tidal flats that do have collapses over time. Locations with rapid infilling of the scar relate to locations with multiple collapses, e.g., at Spijkerplaat (location A) and Ossenisse [location H, *Van Dijk et al.*, 2018a].

Our parametrization differs from earlier attempts to prevent steep slopes of bars in rivers with Delft3D [*Nieuwboer*, 2012]. *Nieuwboer* [2012] applies two strategies to reduce steep slopes in Delft3D; 1) slope avalanching, and 2) slope slumping, in which avalanching stopped deposition of sediment on steep slopes and slumping leads to changing steep slopes to equilibrium. The slope slumping, however, leads to numerically unstable simulations because of large changes in the water levels. Here, no numerical instabilities were observed, because the collapses mainly occurred underwater and water depths are higher in the estuary setting compared to shallow rivers. Furthermore, sediment was not deposited in adjacent cells but spread in the deeper parts of the channel following the slope of the collapsed shoal.

Our parametrization is limited in the correct prediction of the collapses as the original probability prediction of *Van den Ham et al.* [2014] includes also variables for sediment properties, such as grain-size, relative density and the number of mud layers [*Mast-*

bergen and Van den Berg, 2003]. We calculated the probability for a uniform sediment size. Variations in sediment properties form when the channels migrate, forming new shoals on the inner banks whilst collapsing outer banks retreat into the layer-cake of sand and mud of past shoals and marshes [*Dalrymple and Rhodes*, 1995; *Van den Berg et al.*, 1996; *Fagherazzi et al.*, 2004]. Spatial information of the stratigraphy is lacking for most systems, because of the limited field data availability. Even for the well-studied Western Scheldt, a model is used to predict clay availability within the tidal flats [*Dam*, 2017]. It will be of interest for future studies to use multiple fractions, especially to construct a subsurface including variations in sediment properties, such as observed in mud drapes [*Braat et al.*, 2017].

5.2 Implications of shoal margin collapse perturbations on the morphodynamics

The rate of sediment removal and the volume of a single collapse determine the channel dynamics around the collapse. In the less dynamic secondary channels, the sediment is less spread, so that the collapse has less impact on the channel-shoal interactions. Small collapses can be seen as noise to the system, while larger collapses can be seen as a perturbation of the system [*Kleinhans et al.*, 2015]. The shoal margin collapse firstly affects the local bed elevation by depositing sediments into the main channel. Over time the disturbance propagates through the channel network affecting other parts. Our findings correspond partly with the conceptual model described by *Schuurman et al.* [2016a] for disturbances in braided rivers. In the estuary, however, a perturbation in the channel leads to adjustments in the downstream and upstream directions. The dominant direction depends on whether the channel is ebb- or flood-dominant. The migration rate is low for the disturbance but larger than the spatial change rates of the shoals (tidal flats) themselves. Shoals are more or less fixed at their locations [*Hoitink et al.*, 2017; *Leuven et al.*, 2018b].

The initial 10 collapses show that the perturbations lead to excitation of the difference in bed elevation on the long-term (Figure 7). Specifically, the bed elevation difference between the runs increases rapidly after 20 years. After 40 years of morphological development, the modeled bed elevation difference is only explained by less than 10% of the initial collapsed volume. In the case of the scenario with yearly collapses, the modeled bed elevation difference (Figure 8) is explained by 20% of the collapsed volume. We expect this percentage is less because the effects from the disturbances are still growing. Also, the perturbations are less effective because of the smaller collapses, or small perturbations are overprinted by larger ones. In the case of the initial collapses, the perturbation grows over time but besides some deepening of the secondary channel, the channel network remains the same. On the other hand, the yearly collapses change the course of the secondary and main channel at a few locations (Supplementary Animation S1).

In general, the shoal margin collapses change the channel-shoal network by shallowing of the major channels and forming new smaller channels on the tidal flats. The extracted channel network from the final timestep (Figure 9) illustrates the changes between the control run and the yearly collapse, however, these cannot be linked to the collapses themselves. Analysis of the channel depth for the various scales in time shows that the variation in channel depth increases in time, except for the secondary channels (Figure 10). The channel network changes part of the main channel into the secondary channel within the first 5 years for all runs. So, the secondary channel deepens and the main channel becomes shallower (Figure 10a, b). The collapses in the scenario with yearly collapses deepens the secondary, whereas connecting scale channels become generally shallower (Figure 10b, c). A few collapse events can be linked to changes in the channel network depth. For example, the collapses in year 22 result in shallowing of the secondary scale channel (Figure 10b). But changes in the depth of the main and secondary channel network scales are generally not linked to individual collapses. We suggest that the changes in the larger channel scales are the result of multiple collapses that first affected the connecting channel scale. For example, the shallower secondary scale channels after

10 years follow a deepening of the connecting scale channel network that occurred a year before (Figure 10b, c).

The shoal margin collapses do not dynamicise the model as we hypothesized, but do affect the estuary channel-shoal interaction. The most interesting effect is observed near junctions (sills, Figures 7-8), corresponding to the overlapping sediment circulation cells [*Wang et al.*, 1995]. Here, there is less gross sediment transport but the channels shift more often than other parts of the Western Scheldt [*Van Dijk et al.*, 2018a]. This is observed from the DEM of differences for the last decades [*Grasmeijer et al.*, 2013]. Analysis of the development of channel-shoals in the Western Scheldt shows a more dynamic system for the period 1860-1955 [*Dam*, 2017]. These field observations suggest that dynamics of the shoals have decreased in the last decades and that perturbations, such as shoal margin collapses, are efficiently removed in the main and secondary channels and therefore only affect the development at the shallower sills and channel junctions. The role of the junction is significant as this leads to excitation of the disturbance. Disturbances at the junction change the flow direction towards the successive shoal, like the successive bifurcation in a braided river [*Schuurman et al.*, 2016a], but also the flow direction towards the shoal itself as the tidally-averaged flow circulates, i.e., forming a macro cell, around the shoal (Figure 1b). This means that disturbances near a junction would have a larger effect on the channel-shoal interactions. In the field, however, these junctions (sills) are well managed as this is part of the shipping fairway, and therefore its depth is maintained by dredging activities [*Verbeek et al.*, 1998], which means that the role of collapses is interrupted in the field.

The role of the shoal margin collapses might affect the estuary differently compared to dredging and disposal activities, associated with maintaining/ deepening the main channel for navigation. In this study, we have not included dredging and disposal, which would affect our findings. Dredging activities at the toe of the Platen van Ossenisse [Drempel van Hansweert *Groenewoud*, 1997] might lead to deepening and increase the number of shoal margin collapses in the field. This is not included in our simulations. Analysis from disposal strategies also showed that disposal of sediment in the secondary channels takes longer to spread, because of lower sediment transport, and forms a threat for the existence of the multi-channel network [*Meersschaut et al.*, 2004]. Dredged volumes are 10 times larger compared to the volume of shoal margin collapses in the Western Scheldt, and we would argue, therefore, that the role of shoal margin collapses on the morphodynamics in the Western Scheldt is hardly observable. But this study shows that collapses do play a role in the more local, meso-scale morphology, e.g. additional channel-shoal interaction leading to more dynamics. It will be of interest to test what the effect of dredging and disposal is on the stability of the multi-channel network [*Wang*, 2015].

6 Conclusions

Detailed analysis of the large 2014 shoal margin collapse shows that the hydrological and morphological processes around the collapse affect both water levels and the sediment transport direction. Model results show that single shoal margin collapses only affect the local dynamics in the longitudinal direction and dampen out within a year when volumes are small. The extent of far-field effects is sensitive to the grain size of the deposit, where finer sediments are transported further away and settle on the sides of the channel while larger grains are hardly entrained and only eroded during the stronger flood flow. The distribution of the collapsed sediment deposit across the channel disturbs the region around the collapse, where sediment transport is dominantly following the tidally-averaged flow but coarser sediment follows the stronger flood flow. The perturbation by the shoal margin collapses increases channel migration rate, as the deposited sediment pushes the flow against the banks. These results imply that disturbances caused by dredging and dumping may likewise affect the dynamics of channel junctions as well because dredging volumes are at least 10 times larger than the collapsed volumes.

We presented a parametrization for shoal margin collapses and coupled this to the Delft3D model, so that effects of multiple yearly collapses of various sizes on the morphodynamics could be tested. We found that near-field morphodynamics in the channel is slightly affected at a timescale of a year due to increasing bed elevation and changing water levels, but far-field effects controlled by the tidally-averaged flow vectors are negligibly affected by the collapses. When larger disturbances reach the seaward or landward junction at tidal channel junctions over a longer time span, the bed elevation at the junction increases on average and decrease the cross-section geometry of the channel junctions. Here, the perturbation affects the morphology in the longitudinal as well as transverse direction and affects the channel network on a longer term when the flow and sediment distributions into the multiple channels are shifted. The initial collapses have no effect on the long-term channel-shoal morphodynamics, although only 10% of bed elevation difference is explained by the collapsed volume. The yearly collapses resulted in a shallowing of the main channel as they mostly occur along the main channel, and change the channel networks at the various scales. Specifically, the secondary channels become deeper the number of connecting channels increases, because the estuary becomes generally shallower due to the yearly collapses. We conclude that multiple yearly collapses are changing the channel-shoal morphodynamics in estuaries, but that the role of the collapses is limited for heavily dredged systems such as the Western Scheldt. On the other hand, estuaries that are not intensively dredged may not develop oversteepened bar margins with frequent shoal margin collapses.

Acknowledgments

WMvD and MGK were supported by the Dutch Technology Foundation TTW (grant STW-Vici-016.140.316/13710 to MGK), which is part of the Netherlands Organisation for Scientific Research (NWO). MH and MGK were supported by the European Research Council (ERC Consolidator agreement 647570 to MGK). We gratefully acknowledge Marco Schrijver (Rijkswaterstaat), Dick Mastbergen, Marcel Taal (Deltares), Jelmer Cleveringa (Arcadis) and Yves Plancke (WL Antwerpen) for insightful discussions. We greatly thank Willem Sonke, Tim Ophelders, Kevin Verbeek and Bettina Speckman of TU Eindhoven for providing the network extraction tool. Constructive and positive reviews by Ioannis Georgiou, Travis Swanson and one anonymous reviewer, Associate Editor Ton Hoitink, and Editor Giovanni Coco helped to clarify and strengthen the manuscript. Data availability: The data used are reported in the references, figures and supporting information. The Delft3D model software is open source and the code is available from the Deltares website (https://oss.deltares.nl/web/delft3d). All field data from Rijkswaterstaat is publicly available from a variety of web portals or via the service desk (https://www.rijkswaterstaat.nl/zakelijk/open-data). The code for shoal margin collapses is available on the online GitHub repository [*Van Dijk et al.*, 2018b].

References

Ahktar, M. P., N. Sharma, and C. S. P. Ojha (2011), Braiding process and bank erosion in the Brahmaputra River, *International Journal of Sedimentary Research*, *26*, doi: 10.1016/S1001-6279(12)60003-1.

Ashworth, P. J., and J. Lewin (2012), How do big rivers come to be different?, *Earth-Science Reviews*, *114*, 84–107, doi:10.1016/j.earscirev.2012.05.003.

Baar, A., M. B. Albernaz, W. Van Dijk, and M. Kleinhans (2018a), The influence of transverse slope effects on large scale morphology in morphodynamic models, in *Riverflow 2018*, vol. 40, doi:10.1051/e3sconf/20184004021.

Baar, A. W., J. De Smit, W. S. J. Uijttewaal, and M. G. Kleinhans (2018b), Sediment transport of fine sand to fine gravel on transverse bed slopes in rotating annular flume experiments, *Water Resources Research*, *54*(1), 19–45, doi:10.1002/2017WR020604.

Baeyens, W., B. van Eck, C. Lambert, R. Wollast, and L. Goeyens (1997), General description of the scheldt estuary, *Hydrobiologia*, *366*(1), 1–14, doi: 10.1023/A:1003164009031.

Bagnold, R. (1966), *An approach to the sediment transport problem from general physics*, U.S. Geol. Survey. Prof. Paper 422-I.

Beinssen, K., D. T. Neil, and D. R. Mastbergen (2014), Field observations of retrogressive breach failure at the two tidal inlets in Queensland, Australia, *Australian Geomechanics*, *49*(3), 55–64.

Bolle, A., Z. B. Wang, C. Amos, and J. De Ronde (2010), The influence of changes in tidal asymmetry on residual sediment transport in the Western Scheldt, *Continental Shelf Research*, *30*, 871–882, doi:10.1016/j.csr.2010.03.001.

Braat, L., T. Van Kessel, J. R. F. W. Leuven, and M. G. Kleinhans (2017), Effects of mud supply on large-scale estuary morphology and development over centuries to millennia, *Earth Surface Dynamics Discussion*, *5*, 617–652, doi:10.5194/esurf-5-617-2017.

Cancino, L., and R. Neves (1999), Hydrodynamic and sediment suspension modelling in estuarine systems, *Journal of Marine Systems*, *22*, 117–131, doi:10.1016/S0924-7963(99)00036-6.

Canestrelli, A., A. Spruyt, B. Jagers, R. Slingerland, and M. Borsboom (2016), A mass-conservative staggered immersed boundary model for solving the shallow water equations on complex geometries, *International Journal for Numerical Methods in Fluids*, *81*, 151–177, doi:10.1002/fld.4180.

Coleman, J. M. (1969), Brahmaputra River: channel processes and sedimentation, *Sedimentary Geology*, *3*, 129–239, doi:10.1016/0037-0738(69)90010-4.

Crosato, A., and M. S. Saleh (2011), Numerical study on the effects of floodplain vegetation on river planform style, *Earth Surface Processes and Landforms*, *36*, 711–720.

Dalrymple, R., and R. Rhodes (1995), Estuarine dunes and bars, in *Developments in Sedimentology*, vol. 53, pp. 359–422, Elsevier, New York, doi:10.1016/S0070-4571(05)80033-0.

Dam, G. (2013), Harde lagen Westerschelde (in Dutch), *Tech. rep.*, International Marine & Dredging Consultants.

Dam, G. (2017), Lange-termijn sedimentbalans Westerschelde (in Dutch), *Tech. rep.*, SVASEK hydraulics.

Darby, S. E., A. M. Alabyan, and M. J. Van de Wiel (2002), Numerical simulation of bank erosion and channel migration in meandering rivers, *Water Resources Research*, *38*, doi:10.1029/2001WR000602.

De Vet, P. L. M., B. C. Van Prooijen, R. A. Schrijvershof, J. J. Van der Werf, T. Ysebaert, M. C. Schrijver, and Z. B. Wang (2018), The importance of combined tidal and meterological forces for the flow and sediment transport on intertidal shoals, *Journal of Geophysical Research – Earth Surface*, *123*(10), 2464–2480, doi:10.1029/2018JF004605.

De Vriend, H. J., Z. B. Wang, T. Ysebaert, P. M. J. Herman, and P. Ding (2011), Eco-morphological problems in the Yangtze Estuary and the Western Scheldt, *Wetlands*, *31*, 1033–1042, doi:10.1007/s13157-011-0239-7.

Deltares (2009), *Delft3D-FLOW User Manual, Simulation of Multi-Dimensional Hydrodynamic Flows and Transport Phenomena, Including Sediments*, Deltares, Delft, The Netherlands.

Dunbar, J. B., V. H. Torrey, and L. D. Wakeley (1999), A case history of embankment failure: geological and geotechnical aspects of the Celotex levee failure, New Orleans, Louisiana, *Technical report*, US Army Corps of Engineers, Vicksburg, Mississippi, USA.

Fagherazzi, S., E. J. Gabet, and D. J. Furbish (2004), The effect of bidirectional flow on tidal channel planforms, *Earth Surface Processes and Landforms*, *29*, 295–309, doi: 10.1002/esp.1016.

Grasmeijer, B., G. Dam, and M. Taal (2013), Actualisatierapport Delft3D Schelde-estuarium (in Dutch), *Tech. rep.*, International Marine & Dredging Consultants.

Groenewoud, M. D. (1997), Modellering morfodynamisch gedrag van de Drempel van Hansweert (in Dutch), Master's thesis, TU Delft.

Gruijters, S. H. L. L., J. Schokker, and J. G. Veldkamp (2004), Kartering moeilijk erodeerbare lagen in het Schelde estuarium (in Dutch), *rapport NITG 03213B1208*, TNO.

Hoitink, A. J., Z. B. Wang, B. Vermeulen, Y. Huismans, and K. Kästner (2017), Tidal controls on river delta morphology, *Nature Geoscience*, *10*, 637–645, doi: 10.1038/ngeo3000.

Ikeda, S. (1982a), Incipient motion of sand particles on side slopes, *Journal of Hydraulics Division*, *108*(1), 95–114.

Ikeda, S. (1982b), Lateral bed load transport on side slopes, *Journal of Hydraulics Division*, *108*(11), 1369–1373.

Jerolmack, D. J., and C. Paola (2010), Shredding of environmental signals by sediment transport, *Geophysical Research Letters*, *37*(19), doi:10.1029/2010GL044638, l19401.

Jeuken, M. C. J. L. (2000), On the morphologic behaviour of the tidal channels in the Westerschelde estuary, Ph.D. thesis, Universiteit Utrecht.

Khan, N. I., and A. Islam (2003), Quantification of erosion patterns in the Brahmaputra-Jamuna River using geographical information system and remote sensing techniques, *Hydrological Processes*, *17*, doi:10.1002/hyp.1173.

Kleinhans, M. G. (2010), Sorting out river channel patterns, *Progress in Physical Geography*, *34*, 287–326, doi:10.1177/0309133310365300.

Kleinhans, M. G., C. Braudrick, W. M. Van Dijk, W. I. Van de Lageweg, R. Teske, and M. Van Oorschot (2015), Swiftness of biomorphodynamics in Lilliput- to Giant-sized rivers and deltas, *Geomorphology*, *244*, 56–73, doi:10.1016/j.geomorph.2015.04.022.

Kleinhans, M. G., M. Kreveld, T. Ophelders, W. Sinke, B. Speckmann, and K. Verbeek (2017), Computing representative networks for braided rivers, in *33rd International Symposium on Computational Geometry (SoCG 2017)*, *Leibniz International Proceedings in Informatics (LIPIcs)*, vol. 77, edited by B. Aronov and M. J. Katz, pp. 48:1–48:16, Schloss Dagstuhl–Leibniz-Zentrum fuer Informatik, doi:10.4230/LIPIcs.SoCG.2017.48.

Laury, R. L. (1971), Stream bank failure and rotational slump: preservation and significance in the geologic record, *Geological Society of America Bulletin*, *82*, 1251–1266.

Leuven, J. R. F. W., T. De Haas, L. Braat, and M. G. Kleinhans (2018a), Topographic forcing of tidal sand bar patterns for irregular estuary planforms, *Earth Surface Processes and Landforms*, *43*(1), 172–186, doi:10.1002/esp.4166.

Leuven, J. R. F. W., L. Braat, W. M. van Dijk, T. De Haas, J. Cleveringa, and M. G. Kleinhans (2018b), Growing forced bars determine non-ideal estuary planform, *Journal of Geophysical Research – Earth Surface*, *123*(11), 2971–2992, doi: 10.1029/2018JF004718.

Mastbergen, D. R., and R. Schrijvershof (2016), Sedimentatiepatronen Plaat van Walsoorden na plaatval 22 juli 2014 (in Dutch), *Tech. rep.*, Deltares, deltares.

Mastbergen, D. R., and J. H. Van den Berg (2003), Breaching in fine sands and the generation of sustained turbidity currents in submarine canyons, *Sedimentology*, *50*(4), 625–637, doi:10.1046/j.1365-3091.2003.00554.x.

Mastbergen, D. R., G. A. Van den Ham, M. Cartigny, A. Koelewijn, M. De Kleine, J. Hizett, M. Azpiroz, and A. Vellinga (2016), Multiple flow slide experiment in the Westerschelde Estuary, The Netherlands, in *Submarine Mass Movements and Their Consequences, 7th Int. Symp*, *Advances in Natural and Technological Hazards Research*, vol. 41, edited by G. Lamarche, J. Mountjoy, S. Bull, T. Hubble, S. Krastel, E. Lane, A. Micallef, L. Moscardelli, C. Mueller, I. Pecher, and S. Woelz, pp. 241–249, Springer International Publishing, Wellington, New Zealand, doi:10.1007/978-3-319-20979-1.

Maximova, T., S. Ides, J. Vanlede, T. De Mulder, and F. Mostaert (2009a), Verbetering 2D randvoorwaardenmodel. Deelrapport 3: kalibratie bovenlopen (in Dutch), *WL rapporten* 753_09, Flanders Hydraulics Research, Antwerp, Belgium.

Maximova, T., S. Ides, T. De Mulder, and F. Mostaert (2009b), LTV O & M thema Veiligheid - Deelproject 1: Verbetering hydrodynamisch NeVla model ten behoeve van scenario-analyse (in Dutch), *WL rapporten* 756_05, Flanders Hydraulics Research & Deltares, Antwerp, Belgium.

Maximova, T., S. Ides, T. De Mulder, and F. Mostaert (2009c), Verbetering randvoorwaardenmodel. Deelrapport 4: Extra aanpassingen Zeeschelde (in Dutch), *WL rapporten* 753_09, Flanders Hydraulics Research, Antwerp, Belgium.

Meersschaut, Y. M. A., W. R. Parker, J. J. Peters, and Y. M. G. Plancke (2004), A dredging and disposal strategy for managing the Western Scheldt's morphology and ecology, in *WODCON XVII: Dredging in a Sensitive Environment*.

Nicholas, A. P. (2013a), Morphodynamic diversity of the world's largest rivers, *Geology*, *41*(4), 475–478, doi:10.1130/G34016.1.

Nicholas, A. P. (2013b), Modelling the continuum of river channel patterns, *Earth Surface Processes and Landforms*, *38*, 1187–1196, doi:10.1029/2010JF001774.

Nieuwboer, B. (2012), Numerical modelling of Colorado sandbar growth, Master's thesis, TU Delft.

Olsen, N. R. (2003), Three-dimensional CFD modelling of self-forming meandering channel, *Journal of Hydraulic Engineering*, *129*, 366–372, doi:10.1061/(ASCE)0733-9429(2003)129:5(366).

Paola, C., P. Heller, and C. Angevine (1992), The large-scale dynamics of grain-size variation in alluvial basins. I: Theory, *Basin Res.*, *4*, 73–90.

Roelvink, J. A. (2006), Coastal morphodynamic evolution techniques, *Coastal Engineering*, *53*(2–3), 277–287, doi:10.1016/j.coastaleng.2005.10.015.

Schrijvershof, R., and J. Vroom (2016), Effecten van realistische (extreme) stortstrategieën in de Westerschelde (in Dutch), *Tech. rep.*, Deltares.

Schuurman, F., M. G. Kleinhans, and W. A. Marra (2013), Physics-based modeling of large braided sand-bed rivers: bar pattern formation, dynamics, and sensitivity, *Journal of Geophysical Research – Earth Surface*, *118*, 2509–2527, doi:10.1002/2013JF002896.

Schuurman, F., M. G. Kleinhans, and H. Middelkoop (2016a), Network response to disturbances in large sand-bed braided rivers, *Earth Surface Dynamics*, *4*, 25–45, doi:10.5194/esurf-4-25-2016.

Schuurman, F., Y. Shimizu, T. Iwasaki, and M. G. Kleinhans (2016b), Dynamic meandering in response to upstream perturbations and floodplain formation, *Geomorphology*, *253*, 94–109, doi:10.1016/j.geomorph.2015.05.039.

Silvis, F., and M. B. De Groot (1995), Flow slide in the Netherlands: experience and engineering practice, *Canadian Geotechnical Journal*, *32*, 1086–1092, doi:10.1139/t95-107.

Simon, A., and A. J. C. Collinson (2002), Quantifying the mechanical and hydrologic effects of riparian vegetation on streambank stability, *Earth Surface Processes and Landforms*, *27*(5), 527–546, doi:10.1002/esp.325.

Torrey, V. H. (1995), Flow slides in Mississippi riverbanks, in *River, Coastal and Shoreline Protection-Erosion Control. Using Riprap and Armourstone*, edited by C. R. Thorne, S. R. Abt, B. J. Barendt, S. T. Maynard, and K. W. Pilarczyk, pp. 361–377, Wiley, Chichester.

Van de Lageweg, W. I., W. M. Van Dijk, A. W. Baar, J. Rutten, and M. G. Kleinhans (2014), Bank pull or bar push: What drives scroll-bar formation in meandering rivers?, *Geology*, *42*(4), 319–322, doi:10.1130/G35192.1.

Van de Lageweg, W. I., L. Braat, D. R. Parsons, and M. G. Kleinhans (2018), Controls on mud distribution and architecture along the fluvial-to-marine transition, *Geology*, doi:10.1130/G45504.1.

Van den Berg, J. H., C. J. L. Jeuken, and A. J. F. Van der Spek (1996), Hydraulic processes affecting the morphology and evolution of the Western Scheldt estuary, in *Estuarine Shores*, edited by K. F. Nordstrom and C. T. Roman, pp. 157–184.

Van den Berg, J. H., A. Van Gelder, and D. R. Mastbergen (2002), The importance of breaching as a mechanism of subaqueous slope failure in fine sand, *Sedimentology*, *49*(1), 81–95, doi:10.1111/j.1525-139X.2006.00168.x-i1.

Van den Berg, J. H., A. W. Martinius, and R. Houthuys (2017), Breaching-related turbidites in fluvial estuarine channels: Examples from outcrop and core and implications to reservoir models, *Marine and Petroleum Geology*, *82*, 178–205.

Van den Ham, G. A., M. B. De Groot, and D. R. Mastbergen (2014), A semi-empirical method to assess flow-slide probability, in *Submarine mass movements and their consequences*, vol. 37, edited by S. Krastel, J.-H. Behrmann, D. Volker, M. Stipp, C. Berndt, R. Urgeles, J. Chaytor, K. Huhn, M. Strasser, and C. B. Harbitz, Advances in Natural and Technological Hazards Research, Springer International Publishing Switzerland, doi: 10.1007/978-3-319-00972-8.

Van der Wegen, M., and J. A. Roelvink (2012), Reproduction of estuarine bathymetry by means of a process-based model: Western Scheldt case study, the Netherlands, *Geomorphology*, *179*, 152–167, doi:10.1016/j.geomorph.2012.08.007.

Van Dijk, W. M., F. Schuurman, W. I. Van de Lageweg, and M. G. Kleinhans (2014), Bifurcation instability determines chute cutoff development in meandering gravel-bed rivers, *Geomorphology*, *213*, 277–291, doi:10.1016/j.geomorph.2014.01.018.

Van Dijk, W. M., D. R. Mastbergen, G. A. Van de Ham, and M. G. Kleinhans (2018a), Location and probability of shoal margin collapses in a sandy estuary, *Earth Surface Processes and Landforms*, *43*, 2342–2357, doi:10.1002/esp.4395.

Van Dijk, W. M., M. R. Hiatt, J. J. Van der Werf, and M. G. Kleinhans (2018b), Shoal margin collapses in Delft3D, GitHub, doi:10.5281/zenodo.1472212.

van Rijn, L. (1993), *Principles of sediment transport in rivers, estuaries and coastal seas*, 615 pp., Aqua Publications, Oldemarkt.

Van Rijn, L. C. (2007a), Unified view of sediment transport by currents and waves, i: Initiation of motion, bed roughness, and bed-load transport, *Journal of Hydraulic Engineering*, *133*(6), 649–667.

Van Rijn, L. C. (2007b), Unified view of sediment transport by currents and waves, ii: Suspended transport, *Journal of Hydraulic Engineering*, *133*(6), 668–689.

Van Schaick, S. (2015), Morphological development after the July 2014 flow slide on the tidal flat of Walsoorden in the Western Scheldt, Master's thesis, Delft University of Technology.

Verbeek, H., F. T. G. Tank, and M. D. Groenewoud (1998), Drempels in de Westerschelde (in Dutch), *Tech. rep.*, Rijksinstituut voor kust en zee/RIKZ.

Vroom, J., P. L. M. De Vet, and J. J. Van der Werf (2015), Validatie waterbeweging Delft3D NeVla model Westerscheldemonding (in Dutch), *Tech. rep.*, Deltares.

Wang, Z., R. Fokkink, M. de Vries, and A. Langerak (1995), Stability of river bifurcations in 1D morphodynamic models, *Journal of Hydraulic Research*, *33*(6), 739–750.

Wang, Z. B. (2015), Sustainability of the multi-channel system in the Westerschelde under influence of dredging and disposal, in *Scheldt Estuary, physics and integrated management*, pp. 65–70, IAHR.

Wang, Z. B., A. Langerak, and R. J. Fokkink (1999), Simulation of long-term morphological development in the Western Scheldt, in *River, Coastal and Estuarine Morphodynamics*, pp. 367–376.

Whipple, K. X., and G. E. Tucker (1999), Dynamics of the stream-power river incision model: Implications for height limits of mountain rrange, landscape response timescales, and research needs, *Journal of Geophysical Research - Solid Earth*, *104*(B2), 17,661–17,674, doi:10.1029/1999JB900120.

Wilderom, M. H. (1961), Tussen afsluitdammen en deltadijken (in dutch), *Tech. rep.*, Rijkswaterstaat, Vlissingen, The Netherlands.

Wilderom, M. H. (1972), Plaatvallen (in dutch), *OTAR*, *57*(7), 288–305.

Wilderom, M. H. (1979), Resultaten van het vooroeverondervoor langs de Zeeuwse stromen (in Dutch), *Tech. rep.*, Rijkswaterstaat, nota 75.2.

Winterwerp, J. C., M. C. J. L. Jeuken, M. J. F. Stive, and H. J. De Vriend (2000), Lange termijnvisie Westerschelde - Cluster Morfologie (in Dutch), *Tech. rep.*, WL Delft Hydraulics.

Xu, J. (1997), Evolution of mid-channel bars in a braided river and complex response to reservoir construction: an example from the middle Hanjiang River, China, *Earth Surface Processes and Landforms*, *22*, doi:10.1002/(SICI)1096-9837(199710)22:10<953::AIDESP789>3.0.CO;2-S,.

Table 1. Model scenarios

Scenario	Model	Test	duration	comments
1	1	2014 collapse	1 year	see *Van Schaick* [2015]
2	2	initial 10 collapses	40 years	see locations Figure 1a
3	2	yearly collapses	40 years	rule based on *Van Dijk et al.* [2018a]
Sensitivity scenarios				
collapse size	1	100,000 m^3 vs. 1,000,000 m^3	1 year	see Supplementary
grain size	1	100 μm vs. 200 μm vs. 300 μm	1 year	see Supplementary
α_{bn}	1	1.5 vs. 30	1 year	see Supplementary

Table 2. Statistics of the mean μ and standard deviation σ of the depth for the various runs for all network scales.

	μ (m)				σ (m)			
	scenario				Scenario			
Scale	initial	control	2	3	initial	control	2	3
main	-23.91	-26.16	-25.79	-25.73	8.16	10.95	11.13	11.02
secondary	-15.65	-17.41	-17.88	-19.15	7.19	10.87	10.11	11.93
connecting	-10.60	-12.23	-10.62	-12.35	6.60	8.00	5.95	7.09

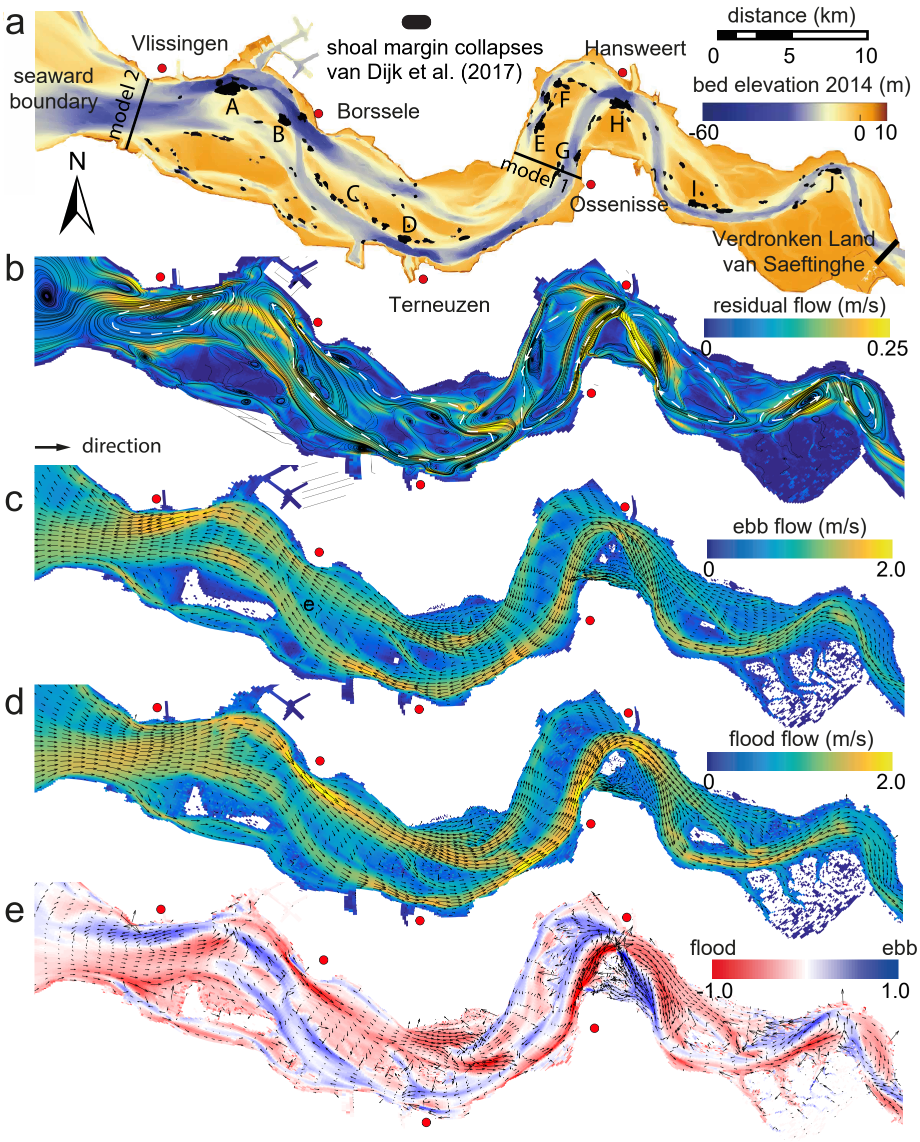

Figure 1. Overview of hydromorphodynamics in the Western Scheldt Estuary. a) Shoal margin collapse locations plotted on a digital elevation model of January 2014 [*Van Dijk et al.*, 2018a]. Seaward boundaries indicated for the two morphological model schematizations in this study. A-J show locations susceptible to shoal margin collapses that are applied in the model scenario with ten initial collapses, and refer to the locations for Figures 5 and 6. b) Streamlines of the tidally-averaged flow of the original NeVla-Delft3D flow model showing circulation cells that correspond to the macro cells indicated in white defined by *Winterwerp et al.* [2000] and *Bolle et al.* [2010]. c) Maximum flow velocity in the ebb-direction from the NeVla-Delft3D model. d) Maximum flow velocity in the flood-direction from the NeVla-Delft3D model. e) Difference (in m/s) between the maximum ebb and maximum flood velocity showing flood dominance in the main channels.

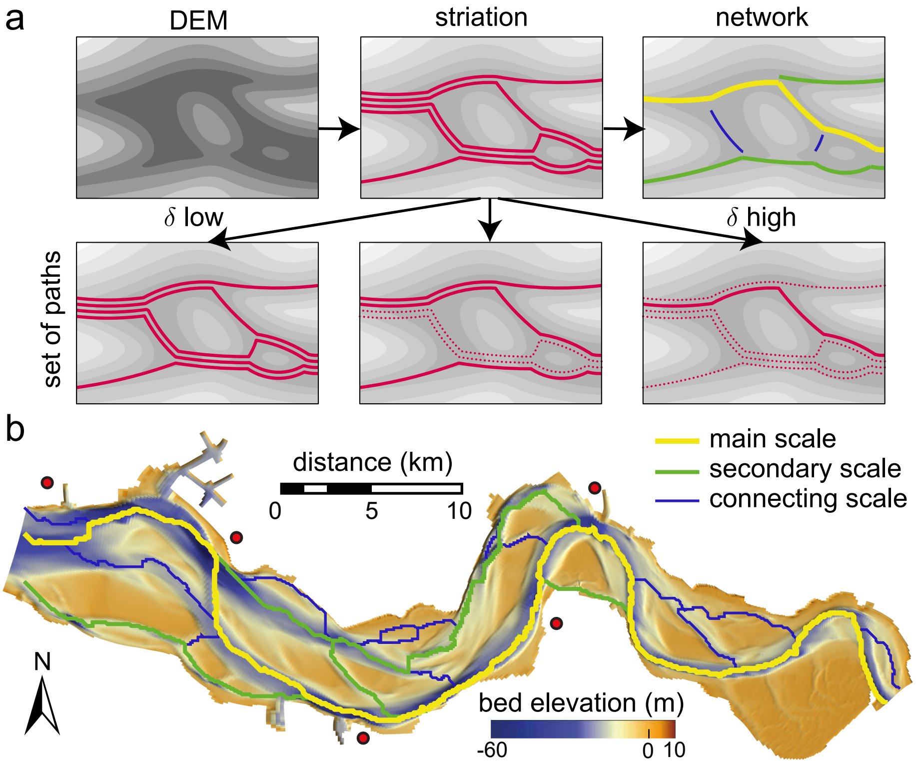

997 **Figure 2.** Illustration of the network extraction approach. a) First, from the DEM, the striation is computed
998 (top). Then, different paths are found (represented by three sand function values, δ, which form the final net-
999 work including the main, secondary and connecting scale. c) Example network for the initial bathymetry of
1000 the Western Scheldt.

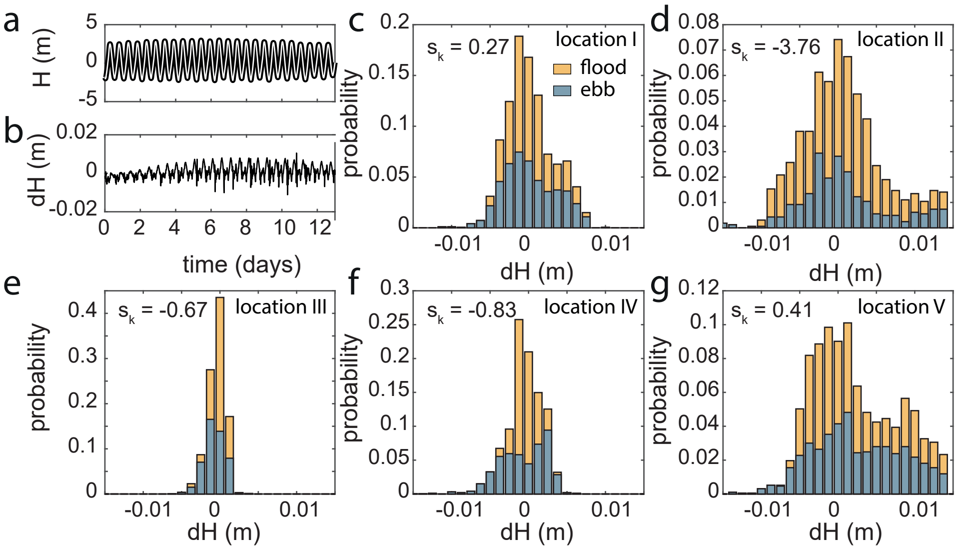

Figure 3. Changes in the water elevation relative to the control run at the 5 surrounding grid cells of the shoal margin collapse of 2014 (locations in Figure 4b). a) Water level at the location of the collapsed sediment deposit (location I) for a simulation without (thick black line) and with the 2014 shoal margin collapse (thin white line on top). b) The difference in water surface elevation at the deposited collapsed sediment is within 1 cm. Positive values show water level rise following the collapse. c) Distribution of water level change shows a slight increase in the water level. Here, s_k indicates if the distribution is skewed to the left (negative) or right (positive) from the mean of the distribution, where the mean is 0 m for all distributions. The two different colors show differences between ebb and flood conditions but no systematic lower or higher water levels. d) The water level generally decreases. e) Seaward there is a slight difference in the water level, whereas f) landward there is more difference as in generally the water level lowers. g) Water level increases on the shoal margin.

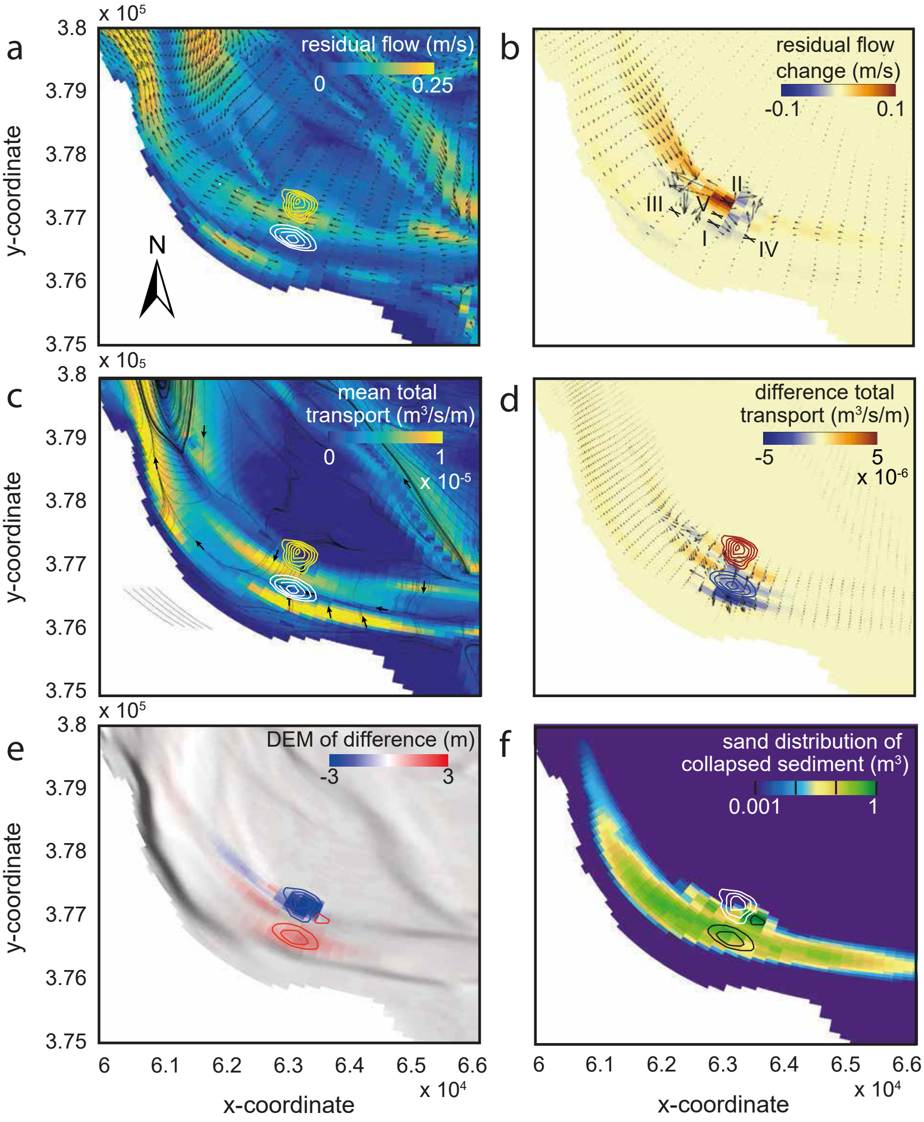

Figure 4. Hydromorphodynamics at a single shoal margin collapse after 1 year compared with a run without the collapse. a) The modeled tidally-averaged flow for the control run shows ebb-dominated flow along the shoal margin collapse of 2014 (yellow), while at the deposit (white) it is around zero. The contour lines were plotted at 1 m elevation intervals. b) Tidally-averaged flow increases along the shoal margin seaward of the collapse and slows down at the collapse. Crosses numbered I-V are the locations for water elevation shown in Figure 3. c) The mean total transport is ebb-dominated at the shoal margin (note vectors), but, as α_{bn} = 30, as a large transverse component into the channel along the Tidal flat of Walsoorden. d) The total transport reduces around the shoal margin collapse. e) The deposited sediment is spread only directly landward and seaward of the collapse, whereas the eroded collapse location remains unfilled. f) Sediment is spread dominantly in the seaward direction in the channel along the vectors of the mean total sediment transport (see Figure 4c).

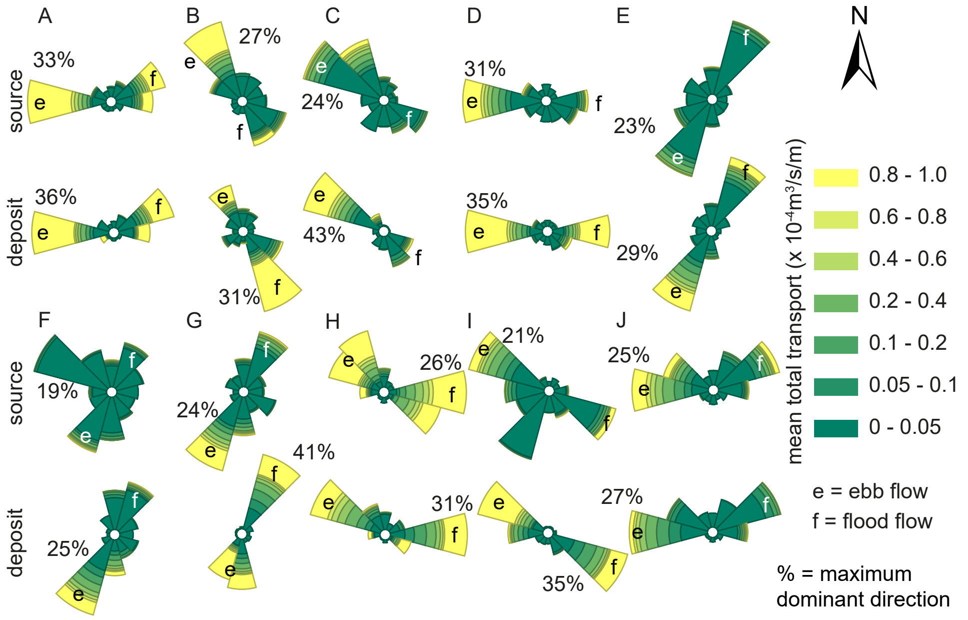

Figure 5. Total sediment transport magnitude and direction for various collapse locations (see locations in Figure 1a) show dominantly ebb and flood flow-related directions for the first year after the collapse. At the shoal margin collapse locations (top rose diagram) less transport is calculated and at some locations, a third dominant direction is observed because of the transverse bed slope effect (see F and I). Sediment transport is generally higher for the deposited sediment (bottom rose diagram). The percentage indicates the maximum duration of the dominant direction.

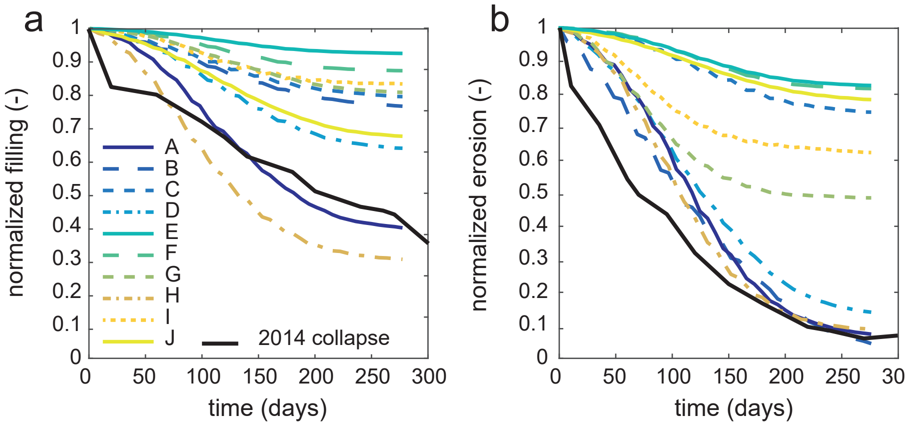

Figure 6. Development of shoal margin collapse scar and deposit volumes normalized by its initial volume at various locations for the Delft3D simulation in the first year (see locations in Figure 1a). The observed shoal margin collapse of 2014, close to the modeled location I, is shown for comparison [see *Van Schaick*, 2015]. a) Filling of the scar varies with location but is never completed within a single morphological year. b) Deposit removal is faster than scar filling. In particular shoal margin collapses in secondary channels develop slowly, e.g. tidal flats of Brouwerplaat (E) and Molenplaat (F), and the less dynamic landward part of the estuary, Verdronken Land van Saeftinghe (J). Wiggles indicate effects of neap-spring tidal cycles.

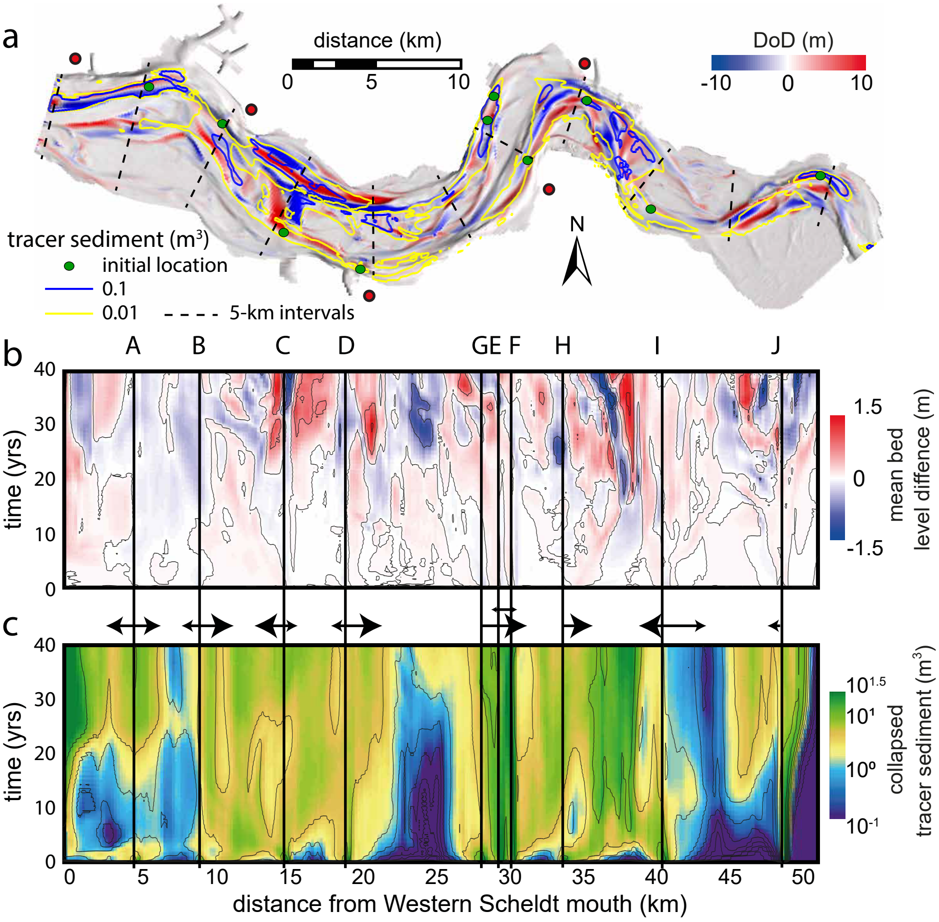

Figure 7. Effect of multiple initial collapses in the Western Scheldt. a) Elevation difference after 40 years between a simulation with and without 10 shoal margin collapses shows that for several locations the perturbation has migrated landward as well as seaward, whereas other collapses hardly migrated over 40 years, e.g., locations E and F (see Figure 1a). The colored contour lines show the spatial distribution of the collapsed material. b) The width-averaged bed elevation difference between the run with and without initial collapses shows some migration of the perturbations but mainly shows cumulative excitation effects after two decades. c) Spatiotemporal distribution of the collapsed sediment, showing spreading in both seaward and landward directions.

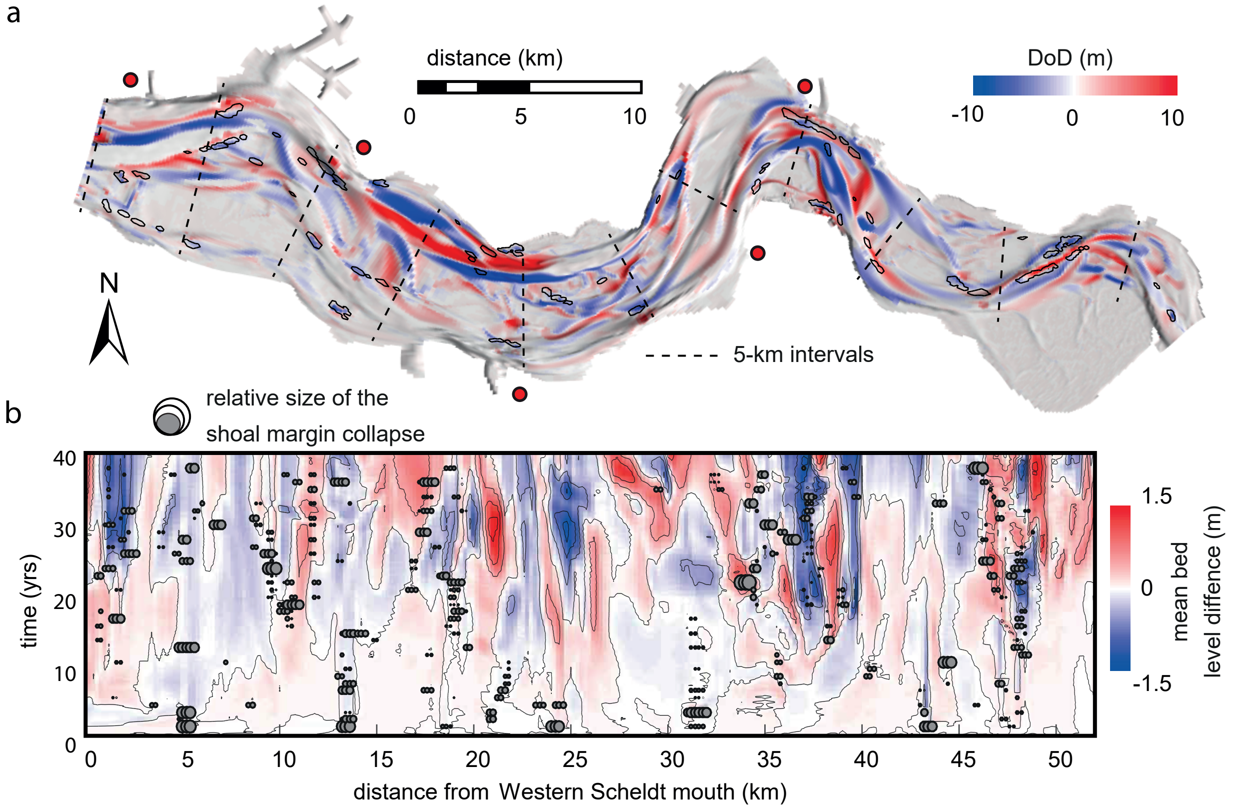

Figure 8. a) Bed elevation difference between a control run and a run with yearly shoal margin collapses (indicated by the contour lines) shows that the entire system is modified, especially at junctions forming ebb-flood channels (landward of location B and at location H). b) The width-averaged bed elevation difference between both runs shows that the location of incision and deposition migrates, excites or dampens depending on the location of the collapse.

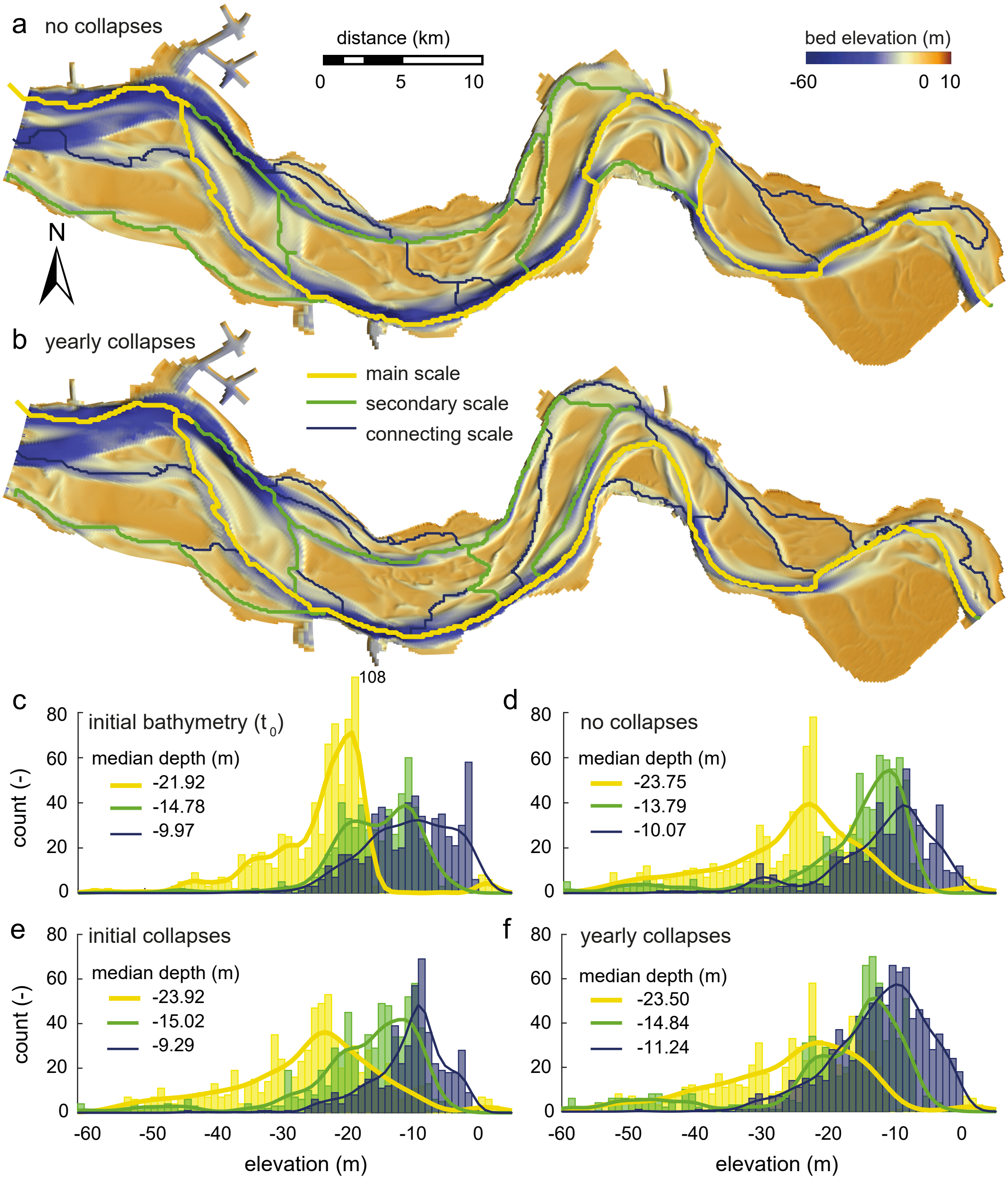

Figure 9. Networks in (a) the control run without collapses and (b) the scenario with yearly collapses, showing that spatial channel shifts and changes in the scale of channels after 40 years of morphological development. c-f) Depth distributions of the channel networks shows a deep initial main channel (c), which becomes shallower when modeled (d). The depth distribution for the run with initial collapses develops towards the control run (e), whereas continuous yearly collapses lead to further shallowing of the main channel in the estuary (f).

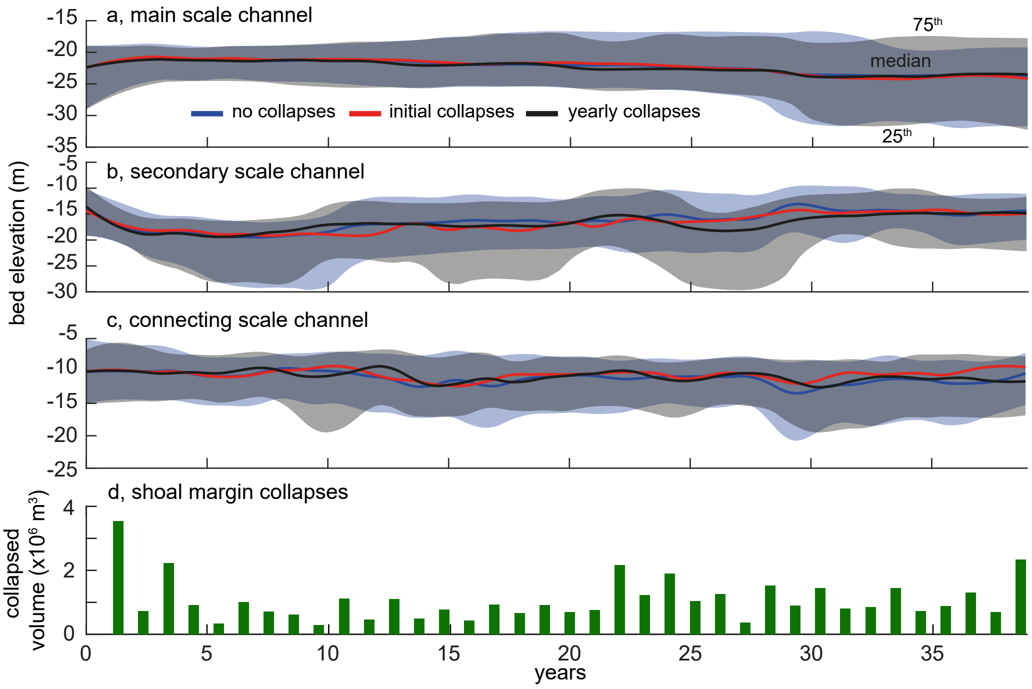

Figure 10. Depth over time for the three model runs illustrating an increasing variation in depth for the various network scales. a) Median depth for the main channel network over time shows minor differences with the control run. b) Secondary channel network deviates after 10 years for the run with yearly collapses. c) Connecting channel network shows a faster response time to collapses. Shading indicates quartiles. Considerable deviations are observed for the yearly collapses at 9, 18 and 30 years and for the initial collapses at 13, 27 and 36 years. d) Time and volume of shoal margin collapses for the scenario with yearly collapses.